JOURNAL OF THERMOPHYSICS AND HEAT TRANSFER
Vol. 21, No. 1, January–March 2007

Surface and Gas Measurements Along a Film-Cooled Wall

Carlos A. Cruz* and André W. Marshall†
University of Maryland, College Park, Maryland 20742

DOI: 10.2514/1.25041

Film cooling is widely used to protect critical sections of propulsion devices from extreme heat loads in the internal flowpath. Many studies have been conducted to formulate scaling laws characterizing the effectiveness of film cooling in a variety of configurations for the development of engineering correlations. There is an emerging demand for detailed measurements near film-cooled surfaces to support computational model development of these complex wall-bounded flows. In this study a unique hot wind tunnel facility was used to perform detailed measurements in a canonical two-dimensional thermally stratified wall-jet configuration. Wall temperature, adiabatic effectiveness, and turbulent flow measurements were performed over a range of carefully controlled inlet conditions. Far-field laboratory effectiveness measurements compare well with previously developed scaling laws; however, the effect of the ratio of mainstream to cooling stream temperature is significantly underpredicted. The micro-thermocouple probe used in this study provided mean flow temperatures and detailed turbulent statistics characterizing the near-wall mixing behavior. The mean flow temperature measurements in the far field demonstrate self-similar behavior whereas fluctuating temperatures indicate fully developed turbulence in the wall layer. The turbulent statistics provided in this study are especially useful for development and validation of computational models of film-cooled surfaces.

Nomenclature

A	=	area
C_p	=	specific heat at constant pressure for the thermocouple bead
f	=	frequency
h_x	=	convective heat transfer coefficient
I_u, I_v	=	streamwise and wall-normal turbulence intensity
k	=	thermal conductivity
l	=	louver thickness
m	=	blowing ratio, $(\rho_c U_c)/(\rho_\infty U_\infty)$
P	=	line between first and last sample point in Eq. (10)
R	=	remaining periodic signal in Eq. (11)
Re_s	=	slot Reynolds number, $U_c s/\nu$
s	=	height of film-cooling injection slot
T	=	mean temperature
T_i	=	instantaneous temperature
T^*_{rms}	=	dimensionless T_{rms} defined by $T_{\text{rms}}/(T_\infty - T_{\text{aw}})$
TR	=	temperature ratio, T_∞/T_c
t	=	time
U	=	streamwise velocity
V	=	wall-normal velocity
δ_T	=	wall-jet thickness defined in Eq. (14)
ε	=	emissivity coefficient
η	=	adiabatic film-cooling effectiveness, defined in Eq. (1)
θ	=	dimensionless instantaneous gas temperature
θ^*	=	dimensionless mean gas temperature
μ	=	dynamic viscosity
ρ	=	density
σ	=	Stefan–Boltzmann constant
τ	=	time constant of thermocouple probe

Subscripts

aw	=	adiabatic wall
c	=	slot film-cooling flow
rms	=	root mean square
0	=	casing
∞	=	mainstream flow

Received 8 May 2006; revision received 21 July 2006; accepted for publication 21 July 2006.

*Ph.D. Student, Department of Aerospace Engineering. Member AIAA.
†Assistant Professor, Department of Aerospace Engineering. Member AIAA.

I. Introduction

FILM cooling is a technique widely used to protect hot section engine components from the extreme thermal loads generated by the combustion process. Whether the coolant is a liquid or a gas, injected through holes or a slot, it is critical to understand the complex flow behavior that dictates the mixing and hence the cooling effectiveness of this thermal protection technique. Advanced computational fluid dynamic (CFD) tools are becoming more accurate in predicting complex flows such as those found in gas turbine combustors or in the thrust chamber of liquid propellant rockets. Engineering CFD analysis requires simultaneous prediction of the combustion and near-wall dynamics for a complete view of the combustion chamber performance. However, this is challenging due to the profound separation of scales in these regions and the computational cost. Both Reynolds-averaged Navier–Stokes (RANS) and large-eddy simulation (LES) wall treatment need to be enhanced to address the aforementioned modeling issues. From this perspective, detailed experimental data are required to provide guidance for future models and the validation of their performance in predicting film-cooling mixing and heat transfer to the wall.

II. Background

A. Previous Work

Film cooling has been studied with great interest during early developments of gas turbine engines. Experimental and analytical efforts were combined to produce simple correlations for estimating the impact of film injection on heat transfer to hot surfaces. In 1946, Wieghardt [1] studied the injection of warm air through a two-dimensional slot as a deicing device by looking at the entrainment of the film by the mainstream as a function of the injection angle for different blowing ratios. He also proposed a similarity expression for the dimensionless gas phase temperature profiles (based on the local adiabatic wall temperature) as a function of the local thermal boundary layer thickness. Measurements and analysis by Hartnett et al. [2] extended Wieghardt's work and provided an expression for film-cooling effectiveness consistent with an expression previously

derived by Tribus and Klein [3]. Stollery and El-Ehwany [4], following earlier developments, derived a simple correlation for slot film-cooling effectiveness based on enthalpy. They mentioned the scatter observed by Hartnett et al. [2] on film effectiveness experimental data is partly due to slightly different slot geometries but mainly due to the fact that the slot Reynolds number was not taken into account in the comparison. This oversight resulted in inappropriate direct comparison of data having different turbulent inlet conditions. All of these correlations are based on the fully developed turbulent boundary layer asymptotic solution and constant gas properties assumption due to small temperature gradients in that region of the flow. Therefore they cannot be applied in the near injection region where large gradients exist, and the turbulent boundary layer is not fully developed. In an attempt to describe the film-cooling effectiveness in the near slot region, Ballal and Lefebvre [5] used Stollery and El-Ehwany [4], and Burns and Stollery [6] analysis and direct measurements of the skin friction coefficient near the slot to describe the effectiveness in this region of interest. After empirical correction for the Reynolds number exponent and the constants, their correlation showed good agreement with experimental data (±5%). For high blowing ratios, they also derived an expression for the effectiveness based on wall-jet theory. Several authors have proposed other simple correlations for the effectiveness. In 1971 Goldstein [7] provided a comprehensive review of those scaling laws.

In 1973 Marek and Tacina [8] suggested that because the adiabatic film-cooling effectiveness is a measure of the mixing of the film, the correlation should depend on axial turbulence intensity in the mainstream through a mixing coefficient C_m. However, they concluded that a constant mixing coefficient along the whole plate leads to a ±30% deviation between the correlation and their experimental data. Later Simon [9] performed a similar analysis, this time, considering the wall-normal turbulence intensities of the mainstream and the slot exit flow. Through a clever wall-jet analysis where he treated separately the jet zone and the mixing zone, Simon was able to describe a 1-D mixing model for the film-cooling problem. This model predicts the film-cooling effectiveness within ±4% of the Marek and Tacina experimental data from which it was developed. Simon also describes a computational method that requires iterations to determine a local mixing parameter equivalent to Marek and Tacina mixing coefficient C_m.

B. Engineering Heat Transfer Modeling

The adiabatic film-cooling effectiveness is a dimensionless form of the adiabatic wall temperature given by

$$\eta = (T_\infty - T_{\text{aw}})/(T_\infty - T_c) \tag{1}$$

where T_{aw}, T_c, and T_∞ are the temperature of the adiabatic wall, the cooling air, and the hot mainstream, respectively. The effectiveness is equal to one at the exit of the slot and then decreases to zero far downstream where the film protection has vanished. The effectiveness depends on several aerothermal parameters such as the velocity ratio U_c/U_∞, the temperature ratio $TR = T_\infty/T_c$, the blowing ratio $m = \rho_c U_c/\rho_\infty U_\infty$, and the slot Reynolds number $Re_s = U_c s/\nu$ based on the velocity of the cooling flow and the slot thickness, s. Although it describes a purely ideal configuration, the adiabatic wall temperature provides an excellent parameter for characterizing performance of film cooling. Goldstein [7] demonstrated that T_{aw} is the appropriate reference temperature for determining heat transfer at a film-cooled wall through evaluation of Newton's law of cooling for a perfectly insulated plate. This reference temperature is typically used with a convective heat transfer coefficient h to determine the convective heat flux $q''_w = h_x(T_{\text{aw}} - T_w)$. To solve for the heat flux (or the wall temperature T_w) using this simple model, the convective heat transfer coefficient h_x and the adiabatic wall temperature T_{aw} need to be determined. Lefebvre [10] recommends using different correlations for the local Nusselt number, Nu_x, depending on the blowing ratio m:

$$Nu_x = \frac{h_x x}{k_c} = \begin{cases} 0.069(Re_s x/s)^{0.7} & 0.5 \le m \le 1.3 \\ 0.10\, Re_s^{0.8}(x/s)^{0.44} & m > 1.3 \end{cases} \tag{2}$$

where k_c is the thermal conductivity of the cooling film.

The adiabatic wall temperature, T_{aw}, can be calculated from Eq. (1) and the appropriate correlation for the film-cooling effectiveness η. For instance, for low blowing ratios in the near slot region Ballal and Lefebvre [5] recommend using the following expression.

For $m \le 1.3$:

$$\eta = 0.6\left(\frac{x}{ms}\right)^{-0.3}\left(Re_s \frac{m\mu_c}{\mu_\infty}\right)^{0.15} \tag{3}$$

For larger blowing ratios Ballal and Lefebvre derived a piecewise correlation based on wall-jet theory.

For $m > 1.3$:

$$\eta = \begin{cases} 1 & x/(ms) < 8 \\ [0.6 + 0.05x/(ms)]^{-1} & 8 \le x/(ms) \le 11 \\ 0.7\left(\frac{x}{ms}\right)^{-0.3}\left(Re_s \frac{\mu_c}{\mu_\infty}\right)^{0.15} & x/(ms) > 11 \end{cases} \tag{4}$$

Having determined the convective heat transfer coefficient and the film effectiveness, the convective heat transfer at a film-cooled wall can then be easily estimated by

$$q''_{\text{conv}} = h_x[T_\infty - \eta(T_\infty - T_c) - T_w] \tag{5}$$

It is worth noting that this approach uses simplifying assumptions such as constant properties, and is mainly limited by the accuracy of the correlations used to determine h_x and η. The mixing model is semi-empirical and does not explicitly account for the effect of turbulence intensity and large disturbances into the prediction of effectiveness. However, it remains a useful method for engineering calculation, especially at the system level. Simon's method [9] for calculating film-cooling effectiveness, η, is a more sophisticated alternative where the effect of turbulence level is taken into account. This approach is based on a wall-jet analysis where an initial region is distinguished from the subsequent fully developed region. The inputs required for predicting the film-cooling effectiveness are the blowing ratio, the temperatures T_c and T_∞, and the wall-normal turbulence intensity both in the slot flow and the mainstream. The reader is referred to Simon [9] for more details on the derivation of the model and its application.

C. CFD Heat Transfer Modeling

With increasing computational power, CFD models are gaining more engineering interest, especially large-eddy simulations models. In a film-cooling numerical simulation study, Zhou et al. [11] have modeled turbulence using a k–ε model with a near-wall low-Reynolds-number k model and also a k–ε model with a wall function. For blowing ratio less than 0.4, their simulation results were in good agreement with the experimental data for velocity profiles and cooling effectiveness. Jansson et al. [12] modeled film cooling through a slot by an algebraic stress model and a standard k–ε model. The numerical results showed excellent agreement with experiments for velocity profiles, but, surprisingly, the comparison for gas temperature profiles showed significant differences. The authors pointed to measurement issues and problems with the way diffusive terms were modeled in the transport equation for temperature to explain these differences.

More recently large-eddy simulations of turbulence have gained interest among the engineering community, even though wall treatment remains a challenge for some complex geometries. Detached-eddy simulation (DES), a promising hybrid technique which combines RANS approach near the wall and LES further away, has been implemented to solve film cooling on a flat plate with injection through discrete holes [13]. The authors of this study noticed a strong anisotropic mixing behavior not captured by RANS but also identified limitations of their simulation due to symmetry conditions imposed in the numerical domain. Although the cost of a

DES is less than that of a DNS, it remains too expensive for engineering applications. One can hope this limitation could be solved by using a coarse grid and appropriate subgrid scale (SGS) models for near-wall mixing and heat transfer.

Previous experimental studies have placed significant emphasis on the wall temperature (i.e., effectiveness). However, as recent numerical studies pointed out, it appears that near-wall temperature profiles and the corresponding wall heat flux are difficult to predict accurately [12]. High quality gas phase and wall temperature measurements under realistic flow conditions (blowing ratio, temperature ratio, slot Reynolds number, turbulence intensity) are needed to help develop and validate emerging near-wall mixing and heat transfer models for film-cooling application.

D. Objectives of the Present Study

This study provides a detailed characterization of the surface and gas phase temperatures at a film-cooled adiabatic wall. Mean and turbulent quantities are presented over a wide range of film-cooling conditions defined by temperature ratios, blowing ratios, and slot Reynolds numbers. The main objectives of this paper are as follows:

1) Present a unique experimental facility for studying near-wall mixing and heat transfer along film-cooled surfaces.

2) Explore under laboratory conditions the performance of engineering film-cooling effectiveness models. Select scaling laws are compared with the current experimental data, and their performance is analyzed while varying parameters such as temperature ratios and blowing ratios.

3) Characterize gas phase thermal mixing through measurement of the temperature field and detailed analysis of temperature statistics including root mean square (rms) and probability density functions (PDF). This information is intended to support model development and validation.

III. Experimental Facility and Diagnostics

A hot wind tunnel facility was specially designed and constructed for the study of near-wall mixing and heat transfer under conditions relevant to gas turbine engines and rocket thrust chamber. In this section the specific components of the facility are described, and the diagnostics are presented along with the data postprocessing technique used to present the experimental results.

A. Hot Wind Tunnel Facility Characteristics

As portrayed in Fig. 1, this wind tunnel is an open circuit system that includes a centrifugal fan, a methane burner, a settling chamber with flow control devices, a two-dimensional convergent section with a contraction ratio of 6:1, and a test section. Downstream of the test section an optimized two-dimensional diffuser reduces pressure losses. A duct connects the exit of the diffuser to a large hood. A high-capacity compressor delivers compressed air that is injected in the test section through a louvered slot to create a tangential film. The hot wind tunnel provides a realistic experimental configuration for investigating heat transfer in rocket thrust chambers and gas turbine engines. Operating conditions are also relevant to real engine conditions with velocity ratios U_c/U_∞ ranging from low values of 0.5 (relevant to rocket engines) and high values up to 3 (relevant to gas turbine engines), absolute temperature ratios T_∞/T_c up to 2, and blowing ratios m ranging from 0.75 (relevant to rocket engines) up to 5 (relevant to gas turbine engines). It should be noted that the peak temperatures in the laboratory configuration are limited when compared with actual engines, particularly rockets (175 K min and 3500 K max). Also the experimental slot injection Reynolds numbers are significantly smaller than those found in propulsion applications; however, they are still in the turbulent regime, ranging from 2000 to 6000.

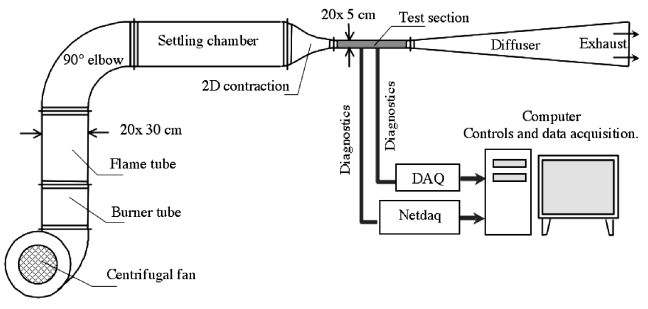

Fig. 1 Layout of the hot wind tunnel facility.

The wind tunnel uses a centrifugal fan driven by a three-phase electric motor. A frequency controller allows selecting the fan rotation speed. Downstream of the fan, a methane inline burner is mounted inside the flame tube. Air bypassing the inline burner provides dilution before entering the 90 deg elbow. Flow detachment and pressure losses at high speeds have been minimized by using turning vanes in the elbow. In the settling chamber, several devices control the flow. First the flow is thermally mixed and homogenized as it passes through a 10-cm-long obstruction made of randomly packed ceramic saddles. This thermal buffer also filters flow inhomogeneities generated by the burner. Then, large scale wall-normal (y) and spanwise (z) turbulent structures are damped as the flow passes through a welded stainless steel honeycomb with characteristic cell diameter of 3.17 mm and length of 15.87 mm. Finally a fine mesh screen is placed before the inlet of the contraction. The pressure drop across the screen homogenizes the velocity profile and reduces the boundary layer thickness [14]. The stainless steel 2-D convergent section with a contraction ratio of 6:1 is mounted downstream of the settling chamber.

The test section is a stainless steel flanged channel 200 × 50 mm cross-section and 500-m-long directly connected to the convergent section. The louvered slot is mounted to the test plate, which is thermally insulated with *Kaowool* boards. The slot geometrical characteristics can easily be modified. For the present paper the slot height s is set to 2.70 mm, and the louver is 0.76 mm thick and 50 mm long. The film flow is injected through discrete holes 3.17 mm in diameter separated by 6.35 mm. Those small jets impinge on the louver to create a film at the exit of the slot. For additional details on the components of the facility the reader is referred to Cruz and Marshall [15].

B. Diagnostics and Measurements

The test facility is equipped with instruments to characterize the mainstream and the cooling film inlet conditions (i.e., velocity and temperature profiles), surface thermocouples to measure the adiabatic wall temperature, and a micro-thermocouple probe to measure the gas phase temperature profiles and access mixing and turbulence scale information.

1. Inlet Characterization

The mainstream inlet conditions are measured with a small size pitot tube equipped with a micro-thermocouple as described in Fig. 2. It includes static and total pressure taps made of 1/16 in outer diameter stainless steel tubes and a 50-μm-diam type K thermocouple insulated in a ceramic tube. Analog temperature and

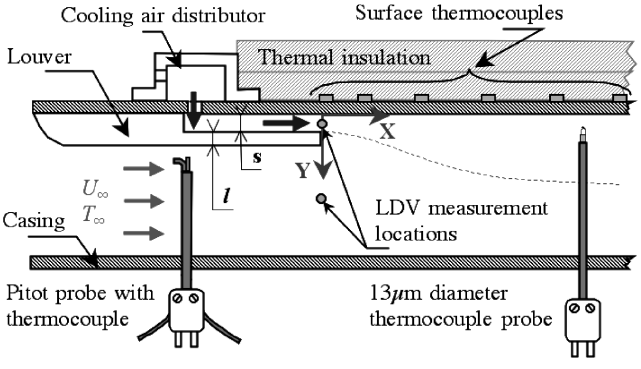

Fig. 2 Test section configuration and diagnostics.

pressure difference are recorded with a Labview DAQ data acquisition board, sampled at 1 kHz and processed to calculate the velocity and the temperature.

The cooling air temperature is measured near the exit of the slot with a 50-μm-wire-diam type K thermocouple, insulated in a ceramic tube. The small probe is inserted through a hole on the test plate and the junction measures T_c, the cooling flow temperature between the louver and the test plate. The average velocity at the exit of the slot is evaluated by mass flow conservation between the flowmeter and the slot exit section.

To make those measurements more useful for CFD model development and validation, turbulent intensity at the slot exit and in the centerline of the mainstream is measured with a single component laser Doppler velocimeter (LDV). This inlet turbulence level is critical for specifying the initial state of mixing. The single component Surepoint LDV system from TSI operates in backscatter mode. It uses a 780 nm wavelength laser. Given the focal length of the optics used here, the probe volume is estimated to be an ellipse 600×200 μm. Because of the high wind tunnel operating temperatures, solid TiO_2 particle seeding was selected for this application with a mean diameter ranging from 0.3 to 1 μm. This LDV system is being refined to also allow measurement of kinematic behavior of the film along the wall.

2. *Wall Surface Temperature Measurements*

The wall surface temperatures are measured with 12 type K surface-mounted thermocouples fixed at different x-locations downstream of the slot. They are attached to the external surface of the test plate to avoid perturbation of the flow. The external surface of the test plate is insulated with *Kaowool* board from Thermal Ceramics. To ensure a good adiabatic wall condition, the efficiency of the thermal insulation is checked experimentally. Preliminary experiments showed the external surface of the insulation to be less than 1°C above the ambient temperature. Using the low thermal conductivity of the insulation ($0.06\ \mathrm{W \cdot m^{-1} \cdot K^{-1}}$) and the temperature gradient across the 1-inch thick board, the heat losses are estimated to be negligible. In fact, using the same heat flux one can estimate the temperature gradient across the stainless steel test plate. Calculations showed this temperature difference is 1 order of magnitude smaller than the accuracy of the thermocouple measurements and validated the measurement technique of the wall surface temperature. Although not used in this study, an infrared camera is also available to measure the wall temperature. This measurement technique provides increased spatial resolution and is more appropriate for evaluating the two-dimensionality of the flow or for measuring wall surface temperatures under more complex cooling configurations (i.e., 3-dimensional).

3. *Gas Temperature Measurements*

Gas phase temperatures are measured with a micro-thermocouple probe as illustrated in Fig. 3. A 13-μm-wire-diam type K thermocouple is threaded through a double-holed ceramic insulation inside a stainless steel tube. The bead extends 2 mm outside the ceramic and the stainless tube to avoid flow disturbances at the measurement location. Given Shaddix [16] recommendations, this distance is also sufficiently long to neglect thermal conduction from contaminating the temperature measurements even under the largest gas phase temperature gradients measured. The probe is inserted through several portholes to measure temperature profiles at selected x-positions downstream of the slot exit and traversed from the wall with a 10 μm-precision traverse. Data were recorded at a 20 kHz sampling frequency.

C. Data Postprocessing

1. *Adiabatic Wall Temperature and Effectiveness Correlations*

Although the test plate is effectively insulated on its backside and conduction losses through the insulation are negligible, axial conduction and radiation from the walls of the test section must also be considered. The axial conduction heat flux has also been determined to be negligible. However, the effects of thermal radiation from the casing to the wall require some correction. Therefore to achieve the adiabatic wall temperature one has only to correct for radiation effects. The correction applied to the data is based on an energy balance between convection and net radiation at the wall [10]. Using the radiosity approach [17] with the measured casing and wall temperatures the net radiation at an axial partitioned wall surface element A_k is given by

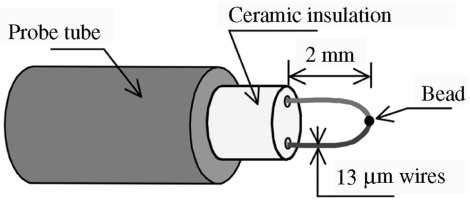

Fig. 3 Details of the 13-μm-diam thermocouple probe.

$$q_k^+ = A_k \varepsilon_w (R_0 - \sigma T_{w,k}^4) \tag{6}$$

where $T_{w,k}$ is the temperature of the wall surface element A_k, ε_w is the wall emissivity, and R_0 is the radiosity of the casing. R_0 is a function of the casing temperature, emissivity and surface, noted T_0, ε_0, and A_0, respectively, and is given by

$$R_0 = \frac{\sigma T_0^4 + (\varepsilon_w - \varepsilon_0 \varepsilon_w)/A_0 \varepsilon_0 \sum_{i=1}^{i=N} \sigma A_i T_{w,i}^4}{1 + (\varepsilon_w - \varepsilon_0 \varepsilon_w)/A_0 \varepsilon_0 \sum_{i=1}^{i=N} A_i} \tag{7}$$

The adiabatic wall temperature is then given by

$$T_{\mathrm{aw},k} = T_{w,k} - q_k^+ / (h_{\mathrm{conv}} A_k) \tag{8}$$

where h_{conv} is the local convective heat transfer coefficient estimated from Eq. (2). In the range of operating conditions considered in present experiments, the moderate convective heat transfer coefficients made the correction small (e.g., less than 7 K) but not negligible. Based upon these corrections, the experimental film-cooling effectiveness η was estimated to have a typical error of $\pm 2\%$.

2. *Gas Temperature*

Because of the small size of the thermocouple probe, radiation and conduction losses are negligible. However, even for a small thermocouple bead of 13-μm-diam, large fluctuations of temperature due to turbulent structures are attenuated at high frequencies due to the thermal inertia of the probe. Noting T_i the actual gas temperature, T_b the bead temperature, and τ the time constant of the bead [with $\tau = m_b C_p / (h_{\mathrm{conv}} A_b)$], it can be shown by a transient heat balance on the bead that

$$T_i = T_b + \tau \frac{\mathrm{d}T_b}{\mathrm{d}t} \tag{9}$$

The thermocouple time constant was estimated by measuring, in the test section, the transient response of the probe to a heating-cooling cycle as described by Marshall [18]. The time constant was between 1.5 and 2.3 ms depending on the relative position of the thermocouple to the wall and the operating conditions. The time constant was used to correct for the thermal inertia of the probe, and recover the power of the fluctuations at high frequencies with a digital compensation technique. The derivative term on Eq. (9), if directly computed by central differencing, becomes contaminated by noise. To avoid this issue, a careful spectral analysis is performed on the signal T_b sampled at 20 kHz for $(t_f - t_i)$ duration. The raw signal is not periodic. To avoid Gibbs phenomenon [19] when applying the fast Fourier transform (FFT), we define the line $R(t)$ joining the first and last data point of T_b by

$$R(t) = T_b(t_i) + (t - t_i)[T_b(t_f) - T_b(t_i)]/(t_f - t_i) \tag{10}$$

We then define $P = T_b - R$, a periodic signal on $[t_i, t_f]$. Substituting into Eq. (9) results in

$$T_i = P + \tau\frac{dP}{dt} + R + \tau\frac{dR}{dt} \tag{11}$$

The two last terms on the right-hand side of Eq. (11) are analytic functions: R is a line and its derivative is a constant. The first and second terms are determined from measurements and consequently have embedded electronic noise. To minimize electronic noise these two terms are treated in Fourier space resulting in

$$\mathcal{F}\left(P + \tau\frac{dP}{dt}\right) = (1 + j\tau\omega)\mathcal{F}(P) \tag{12}$$

where $\mathcal{F}$ is the Fourier transform operator, $\omega = 2\pi f$ is the angular frequency, and j the complex number defined by $j^2 = -1$. After the transform the derivative of the signal is easily determined from the complex product in frequency space. A low-pass filter $\mathcal{L}_{fc}$ with frequency cutoff f_c (defined by a signal-to-noise ratio of 5:1 across the entire frequency range) is then applied along with the inverse Fourier transform yielding the actual filtered gas temperature signal,

$$T_i = \mathcal{F}^{-1}\{\mathcal{L}_{fc}[(1 + j\tau\omega)\mathcal{F}(P)]\} + R + \tau\frac{dR}{dt} \tag{13}$$

Further analysis was performed on the gas phase temperature measurements to obtain the mean, the root mean square, and the probability density function.

D. Test Matrix

Seven experimental cases with blowing ratios ranging from 0.66 to 2.29 are considered in this study. Experimental conditions for Cases 1–7 are summarized in Table 1 highlighting the main parameters influencing film-cooling effectiveness. Temperature ratios TR vary from 1.35 to 1.62 and slot Reynolds number from 1787 to 5171. U_∞ is the velocity of the mainstream and U_c is the average velocity across the slot at the exit location.

The inlet turbulent conditions are measured at the exit of the slot at $y/s = 0.5$ and in the mainstream at $y/s = 10$ as mentioned in Fig. 2. The exit of the slot is located 12.5 cm downstream of the contraction exit. In the mainstream the streamwise and wall-normal turbulence intensities are defined by $I_{u,\infty} = U_{\infty,\mathrm{rms}}/U_\infty$ and $I_{v,\infty} = V_{\infty,\mathrm{rms}}/U_\infty$, respectively. In the film stream the streamwise and wall-normal turbulence intensities are defined by $I_{u,c} = U_{c,\mathrm{rms}}/U_c$ and $I_{v,c} = V_{c,\mathrm{rms}}/U_c$, respectively. These inlet turbulence quantities are presented in Table 2.

IV. Results Analysis

A. Thermal Characteristics of a Film-Cooled Surface

Measurements of the adiabatic effectiveness have been performed over a large range of operating conditions. The blowing ratio and the temperature ratio have been previously identified as important parameters governing film-cooling performance. Figure 4 shows comparisons between predicted and measured adiabatic effectiveness. In Fig. 4a data are compared to the boundary-layer-based correlation Eq. (3). For higher blowing ratios, in Fig. 4b, data are compared to the wall-jet based correlation Eq. (4). For low to moderate blowing ratios, Fig. 4a, comparison of the measured and predicted effectiveness in Case 4 demonstrates excellent agreement far away from the point of injection, but relatively poor agreement in the region of the flow where the effectiveness decays rapidly. The

Table 1 Operating conditions of the experimental cases

Case	T_∞, K	T_c, K	U_∞, m/s	U_c, m/s	TR	m	Re_s
1	428	318	24.4	12.0	1.35	0.66	1851
2	515	331	25.6	12.5	1.56	0.76	1787
3	515	319	26.7	21.2	1.62	1.28	3245
4	413	306	23.0	22.0	1.35	1.29	3605
5	429	309	19.9	28.8	1.39	2.00	4663
6	431	306	20.0	31.5	1.41	2.22	5171
7	429	306	17.5	28.6	1.40	2.29	4697

Table 2 Inlet turbulence intensities for Cases 3 and 6

Case	$I_{u,\infty}$, %	$I_{u,c}$, %	$I_{v,\infty}$, %	$I_{v,c}$, %
3	1.7	19.0	1.7	3.5
6	1.6	27.0	1.6	5.0

effectiveness is underpredicted in this region. The correlations based on turbulent boundary layer theory tend to provide a better prediction far from the slot exit. A comparison of Cases 1 and 4 illustrates the effect of blowing ratio. In this range of blowing ratio, increasing the blowing ratio, from Case 1 to 4, increases the effectiveness. This effect is captured well in the scaling laws used in the correlations. Alternatively, increasing the temperature ratio has the opposite effect of decreasing the effectiveness as demonstrated when comparing Cases 4 and 3. However, the temperature ratio effect appears to be significantly underpredicted by the scaling laws. The impact of the correlation underprediction of the temperature ratio effect can be significant, even leading to incorrect prediction of trends as demonstrated by comparing Cases 1 and 2. Increasing both the blowing ratio and the temperature ratio from Case 1 to Case 2 results in a net reduction in the measured effectiveness because of the importance of the temperature ratio effect. However, the correlation predicts the trend incorrectly and suggests an increase in the effectiveness from Case 1 to Case 2 owing to the weak temperature ratio formulation used in the correlation.

At blowing ratios higher than 1.3, correlations based on turbulent boundary layer theory are not applicable because the underlying assumption on the flow pattern does not hold. In the range $m > 1.3$, Lefebvre [10] recommends the use of correlations based on turbulent wall-jet theory given in Eq. (4). In Fig. 4b for blowing ratios equal to

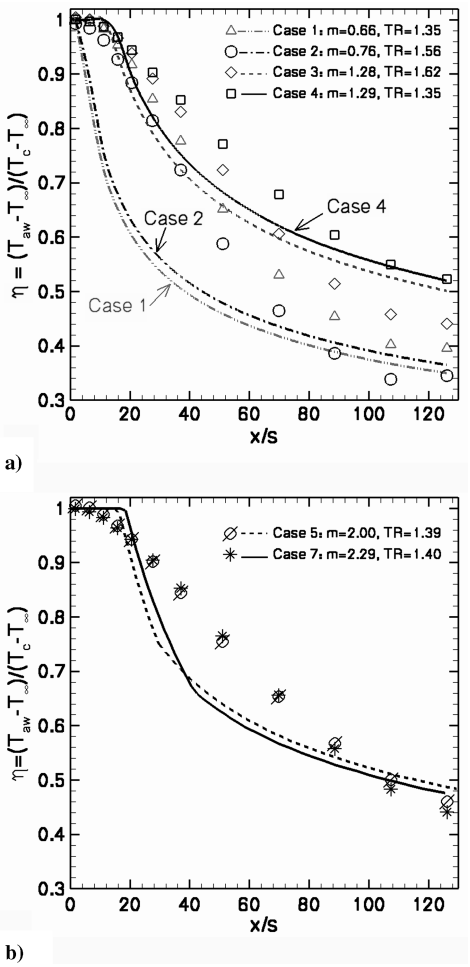

Fig. 4 Experimental data compared to effectiveness correlations based on a) boundary layer analysis, Eq. (3), and b) on wall-jet theory, Eq. (4). (Symbols) experimental data; (lines) predictions.

2.00 and 2.29, measured effectiveness are compared to the correlation based on wall-jet theory. For Case 5 ($m = 2.00$), comparison of measured and predicted effectiveness shows good agreement far from the exit of the slot, but the decay of effectiveness is overpredicted by the correlation for x/s in the range between 30 and 80. The effect of blowing ratio is analyzed by comparing measured and predicted effectiveness for Cases 5 and 7, for which the temperature ratios are similar (i.e., 1.39 and 1.40, respectively). Experimental data show that increasing the blowing ratio increases the effectiveness slightly in the near-field region ($x/s < 70$), while reducing the effectiveness slightly in the far field. The same trend is predicted by the correlation when increasing the blowing ratio, but the performance for Case 7 becomes inferior to that of Case 5 closer to the injection point at x/s equal to 40, rather than 70 as suggested by experimental data.

The effect of blowing ratio is highlighted in Fig. 5 where the effectiveness from experimental data is plotted versus the blowing ratio m, for m ranging between 0.66 and 2.29. Four experimental conditions, Cases 1, 4, 5, and 7, were selected in this range of blowing ratios. These cases have similar temperature ratios; consequently this effect is neglected in this comparison. The change in effectiveness due to the blowing ratio is reported at four x/s locations downstream of the slot exit: one in the near-slot region, one in the far-field region, and two intermediate locations. Blowing ratio trends are reflected in the scaling laws. However, it is worthwhile to evaluate the experimental data, especially because the previous analysis revealed that the scaling laws consistently underpredict the effectiveness at intermediate locations. In the near-slot region (i.e., $x/s = 1.8$) the effectiveness is nearly independent of the blowing ratio and close to unity. At this location the film very close to the wall has not yet been perturbed by the mixing structures initiated at the interface of the two layers. The effectiveness is essentially unchanged at this location even with the distinct inertial differences (and resulting shear) between the layers associated with large blowing ratio. Further downstream at x/s of 37, the effectiveness increases with an increase in the blowing ratio but rapidly reaches a plateau for m around 1.29. As m increases the cooling flux increases which explains enhanced cooling effectiveness at every location downstream of the slot for low to moderate blowing ratios ($m < 1.3$). This trend is well captured by the scaling law in Eq. (3).

However, at higher blowing ratios ($m > 1.3$), the impact of the blowing ratio changes and depends on the location downstream of the slot as demonstrated in Fig. 5. Near the slot exit the effectiveness is virtually independent of the blowing ratio. But further downstream ($x/s \geq 70$) the effectiveness decreases with increasing blowing ratio. At those blowing ratios the intense shear mixing associated with large m competes with and ultimately overpowers the increased cooling flux resulting in a net reduction of cooling effectiveness with increasing m. The shear mixing results in penetration or sweeping of hot gases into the film layer close to the wall despite increases in the cooling flux. This reduction in effectiveness becomes more apparent at downstream locations where the mixing structures, which act to destroy the film, have had sufficient time to develop. For instance at x/s equal to 70, an increase in the blowing ratio results in a higher effectiveness for blowing ratio less than 1.29, but a similar increase at blowing ratios greater than 1.29 results in a lower effectiveness. A more pronounced trend is noticed in the far field for x/s equal to 126. The inverse effect of m at high blowing ratios on the effectiveness is reflected in Eq. (4).

The importance of turbulent mixing in determining the film decay is apparent from the adiabatic wall effectiveness results. Recently Simon [9] developed a model for the film-cooling effectiveness where the initial state of turbulence is taken into account. This model requires an estimate of the turbulence in the freestream and at the exit of the slot through the turbulence intensity based on the rms of the wall-normal velocity component, $I_{v,c} = V_{c,\mathrm{rms}}/U_c$ and $I_{v,\infty} = V_{\infty,\mathrm{rms}}/U_\infty$. Cases 3 and 6, with blowing ratios of 1.28 and 2.22, respectively, were selected for analyzing the performance of Simon's model as shown in Fig. 6. The wind tunnel was designed to obtain a well-characterized freestream with low turbulence intensity levels. This has been confirmed by LDV measurement at the inlet of the test section where the turbulence intensity $I_{v,\infty}$ is 1.7% and 1.6% for Cases 3 and 6, respectively. The slot wall-normal turbulence intensity, $I_{v,c}$, is also reasonably small and was measured to be 3.5% and 5.0%, for Cases 3 and 6, respectively. Computed effectiveness data are compared to experimental data. The comparison for both cases shows good agreement, particularly for x/s less than 70, region where previous power law correlations failed to predict the effectiveness with acceptable accuracy. In this region, the magnitude and slope of the decay of effectiveness is well captured by the model. However, further downstream ($x/s > 70$) the model does not perform quite as well. For Case 6, Simon's model overpredicts the effectiveness whereas for Case 3 there is a small underprediction. The reader is reminded that Simon's model was developed and validated based on Marek and Tacina experimental data for which the maximum x/s location is 34. Simon used these near-field data to evaluate the constants of the model, leaving the model performance in the far field unvalidated. However, comparison with present data provides an indication of the model performance in the far field.

B. Film Mixing Characteristics

From the preceding discussion it is apparent that film cooling at high blowing ratios is characterized by intense turbulent mixing near the wall responsible for the streamwise decay of film-cooling effectiveness. To characterize the thermal mixing behavior, Case 6 ($m = 2.22, TR = 1.41$) is considered. The thermal mixing of the film is analyzed in terms of gas temperature statistics. The gas temperature measurements provide flow details yielding insight into the wall effectiveness behavior.

1. *Mean Temperature Profiles*

In Fig. 7a instantaneous realizations of the temperature are averaged to obtain the mean temperature profiles at four locations

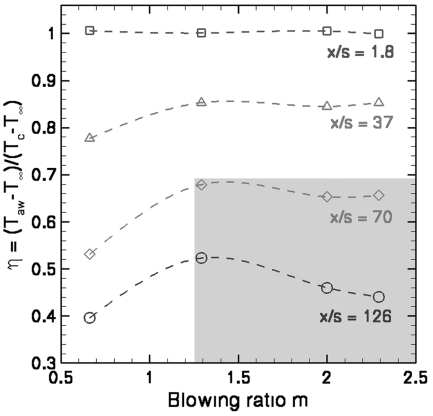

Fig. 5 Effect of blowing ratio m on the effectiveness η; (symbols, lines) experimental data.

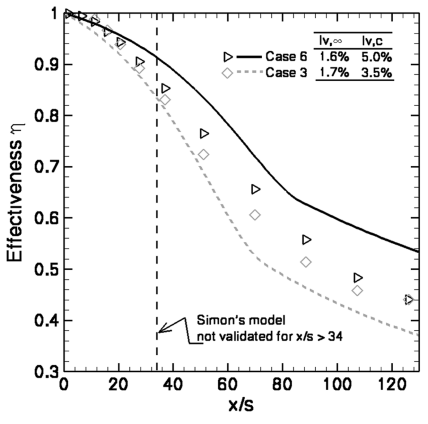

Fig. 6 Performance of Simon's model for predicting the effectiveness.

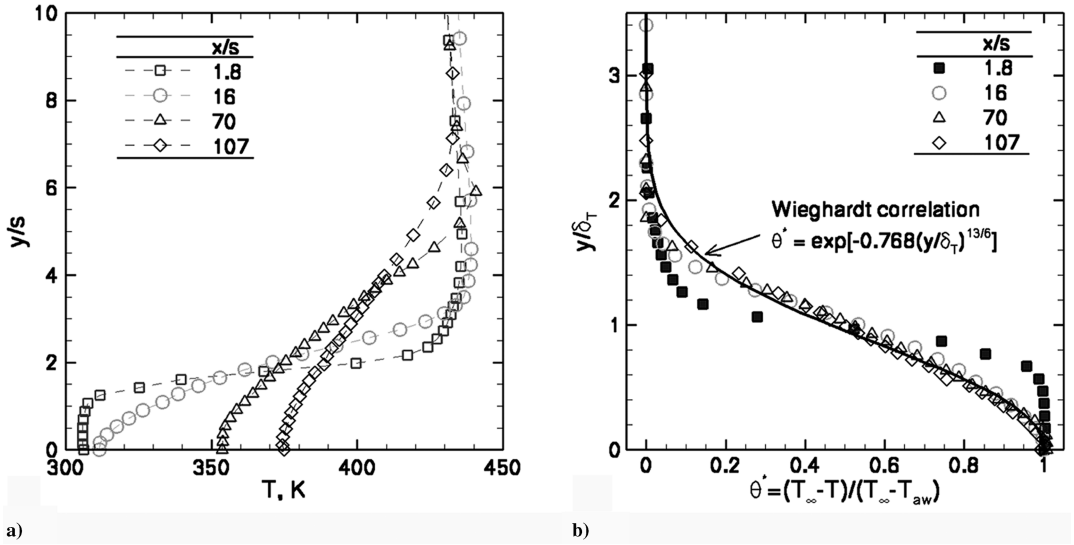

Fig. 7 Case 6: a) Mean gas temperature profiles at selected x/s locations; b) dimensionless profiles and comparison with Wieghardt correlation. δ_T, the thermal boundary layer thickness, is equal to 5.0, 5.4, 8.6, and 9.4 mm, respectively, for x/s of 1.8, 16, 70, and 107.

downstream of the slot exit defined by x/s of 1.8, 16, 70, and 107. For each profile the closest distance from the wall is approximately equal to the diameter of the thermocouple wire, i.e., 13 μm. Gas temperatures at those locations agree very well with measured wall temperatures. The profiles evolve from their respective wall temperature to the freestream temperature, T_∞, and present an inflection point that varies with the streamwise position. At the closest location from the slot exit ($x/s = 1.8$), the inflection point is located at y/s of about 1.6. This profile shows ideal adiabatic behavior at the wall with a zero-gradient zone for y/s less than 0.8. The initial mixing zone is clearly visible with large temperature gradients from y/s of 1.0 to 2.5. At x/s equal to 16, the shape of the profile changes with a less-pronounced inflection point and a mixing zone penetrating closer to the wall. Further downstream the mixing is more distributed across the profile because the gradients near the inflection points are less pronounced and the freestream temperature is reached further away from the wall. It is worth noting the adiabatic wall condition remains excellent at the two extreme streamwise locations.

Mean gas temperature profiles were integrated to evaluate the thermal boundary layer thickness, δ_T, as defined by Wieghardt [1]:

$$\delta_T = \int_0^\infty \theta^*(y)\,\mathrm{d}y = \int_0^\infty \frac{T_\infty - T(y)}{T_\infty - T_{\mathrm{aw}}}\,\mathrm{d}y \tag{14}$$

In Fig. 7b the mean gas temperature profiles are plotted in their dimensionless form, $\theta^* = (T_\infty - T)/(T_\infty - T_{\mathrm{aw}})$, vs the dimensionless wall-normal distance, y/δ_T. These experimental data are also compared to Wieghardt [1] correlation $\theta^*(y) = \exp[-0.768(y/\delta_T)^{13/6}]$. The thermal boundary layer thickness δ_T is equal to 5.0, 5.4, 8.2, and 9.4 mm, for streamwise locations x/s equal to 1.8, 16, 70, and 107, respectively. These initial calculations show the thermal boundary layer grows linearly with the streamwise distance, a feature consistent with classical wall-jet theory although the growth rate defined by $\mathrm{d}\delta_T/\mathrm{d}x = 0.016$ is smaller than the growth rate based on the location of $y_{1/2}$ in the velocity profile as defined by Launder and Rodi [20]. At $x/s = 1.8$, the profile closely resembles a step function with shear effects having insufficient time to significantly adjust the profile. However, further downstream ($x/s = 16$), experimental data tend to approach the correlation profile. In fact, at $x/s = 70$, the mean temperature measurements match the correlation within 2% except for a few points, demonstrating that a self-preserving temperature profile is reached.

2. *Film Mixing and Statistics Information*

Higher order statistic moments (rms, skewness, and flatness) are computed to provide a precise description of the mixing and the PDFs are evaluated to further characterize the mixing process responsible for the decay of cooling effectiveness. Evolution of the temperature statistics provides quantitative insight into the flow behavior and mixing process between the mainstream and the film layer at the wall. The rms of the temperature is nondimensionalized by the expression $T^*_{\mathrm{rms}} = T_{\mathrm{rms}}/(T_\infty - T_{\mathrm{aw}})$, where T_{aw} is the local adiabatic wall temperature. This dimensionless rms of temperature, T^*_{rms}, is plotted in Fig. 8 against y/δ_T axis at the same four streamwise locations previously selected. Close to the slot exit, at $x/s = 1.8$, T^*_{rms} is nearly uniform in the film layer and in the freestream flow. At this location, the peak of T^*_{rms} occurs at y/δ_T of about 1.0, corresponding to the position of maximum mean temperature gradient. Further downstream at $x/s = 16$, the mixing region intensifies and grows in size. For $x/s \geq 70$ the dimensionless rms profile flattens, indicating more intense mixing and penetration of mainstream fluid. The presence of a nearly uniform T^*_{rms} value in the film suggests that a fully turbulent film layer has developed. The development of the fully turbulent film layer is consistent with the previously discussed self-similar profiles. The nearly flat $T^*_{\mathrm{rms}} = 0.1$ profiles, from $y/\delta_T = 0.1$ to 1.4, reflect the intense mixing occurring in the flow.

In Fig. 9 PDFs of the gas temperature are presented at selected streamwise and wall-normal locations. The selected streamwise locations include a position near the slot exit ($x/s = 16$) and two positions further downstream at x/s equal to 70 and 107. At each x/s location the selected wall-normal positions include the point of maximum rms (i.e., $y/\delta_T = 1.00$), a position close to the wall at y/δ_T equal to 0.09 and a position near the mainstream but still in the mixing layer at y/δ_T equal to 1.84. To allow direct comparison, the PDFs were obtained using the same bin size. The PDFs are plotted against a dimensionless instantaneous temperature defined by $\theta_i = (T_\infty - T_i)/(T_\infty - T_c)$. This dimensionless temperature is consistent with the definition of the cooling effectiveness η given in Eq. (1). Although θ_i and η have a similar form, θ_i is not strictly bounded between 0 and 1 because it includes instantaneous realizations of temperature that can be larger than mean values of T_∞ or smaller than mean values of T_c. Consistent with the effectiveness, a large θ_i corresponds to a gas temperature close to the coolant temperature, T_c, and a small θ_i represents a gas temperature close to the hot mainstream temperature T_∞. At x/s equal to 16, the near-wall PDF ($y/\delta_T = 0.09$) presents a large flatness and skewness toward low θ_i corresponding to higher temperature. This PDF is characteristic of near-wall thermal mixing behavior, where large fluctuations of temperature are most likely to be positive. Further away form the wall, at $y/\delta_T = 1.00$, the PDF resembles a Gaussian profile with skewness and flatness factors about (0.24, 2.71), respectively. This PDF is representative of intense mixing as mentioned before when analyzing the rms. Near the edge of the

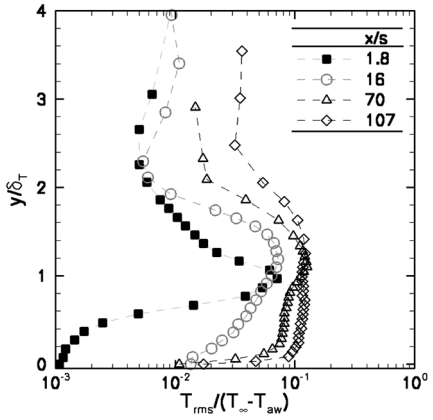

Fig. 8 Case 6, profiles of dimensionless rms of temperature T^*_{rms}.

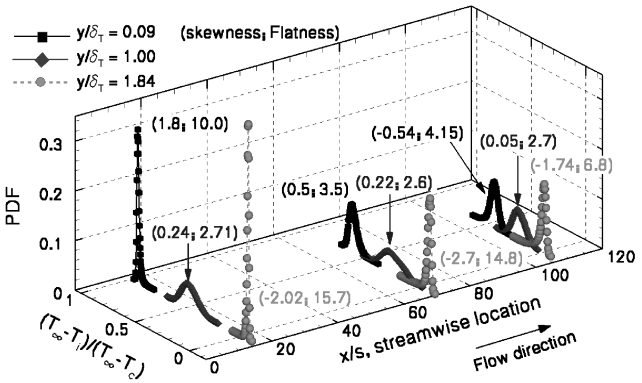

Fig. 9 Case 6, PDFs of the gas temperature at selected x/s and y/δ_T locations, plotted on a dimensionless temperature scale $(T_\infty - T_i)/(T_\infty - T_c)$. Labels in parentheses are (skewness; flatness).

mixing layer, at $y/\delta_T = 1.84$, the shape of the PDF presents a spiky shape with a significant tail towards high θ_i (i.e., low temperature) which is characteristic of PDFs with negative skewness and large flatness. Further downstream at x/s equal to 70 and 107, similar observations can be made. However, as indicated by the decreasing flatness near the wall and the edge of the film, the PDFs become broader, which indicates a more intense mixing directly correlated to the film decay. The shape of the PDFs remains skewed but the skewness tends to decrease faster near the wall. In the far field at $y/\delta_T = 1.00$, the temperature distribution becomes nearly Gaussian indicating intense mixing.

The interpretations of these data provide detailed quantitative information with regard to the state of the film thermal mixing near the wall and its evolution along the streamwise direction. These mixing statistics are useful for high-fidelity CFD model validation.

V. Conclusions

Measurements of the adiabatic effectiveness were made in a hot wind tunnel under laboratory conditions and well-characterized inlet conditions. Experimental data were obtained over a range of operating conditions. These experimental data were compared to previously developed correlations for the effectiveness based on boundary layer or wall-jet theories and to Simon's model based on wall-jet theory. The comparison showed that for low to moderate blowing ratios the boundary-layer-based correlation consistently underpredicts effectiveness in the midfield region. In addition, this comparison revealed that the correlation is not sensitive enough to temperature ratio. At higher blowing ratios, experimental data were compared to a wall-jet-based correlation. The wall-jet-based correlation showed similar weakness in accurately predicting the effectiveness near the slot. However, relatively good agreement is achieved in the far field. Simon's model performance is superior to the simple correlations in the midfield. Although this model was not validated in the far field due to a lack of experimental data, the present work shows that it provides a reasonable estimate of the effectiveness in this region. Unfortunately Simon's model requires a good estimate of the inlet turbulence intensities that are often unknown in the design process of a new engine.

The micro-thermocouple used in this study provided interesting statistical information about the turbulent flow near a film-cooled wall. The complexity of the flow behavior and the short time scales associated with the turbulent structures generated at those speeds are real experimental challenges. The short response time associated with the probe allowed capturing the structures present in the flow. High-quality temperature profiles were measured under an excellent adiabatic wall condition. Starting at 16 slot heights downstream of the slot exit mean gas temperature profiles agreed well with Wieghardt's similarity expression [1], demonstrating the self-similar behavior of the mixing region. Gas phase temperature fluctuation statistics provided quantitative information about the development of the flow, in particular the mixing region and its growth. Nondimensionalized temperature rms profiles showed development of a self-similar profile further downstream of the slot exit. PDFs along the plate in the mixing region provide more detail regarding the thermal mixing development of the film, which can be directly related to the cooling effectiveness. These detailed measurements with well-defined inlet conditions provide information to support CFD model development and validation in a way not possible from existing scaling laws. To complement the current study, near-wall particle image velocimetry diagnostics are being developed for a complete view of turbulent transport near film-cooled surfaces.

Acknowledgments

This work has been sponsored by the Space Vehicles Technology Institute, grant NCC3-989, one of the NASA University Institutes, with joint sponsorship from the Department of Defense. Appreciation is expressed to Claudia Meyer of the NASA Glenn Research Center, program manager of the University Institute activity, and to John Schmisseur and Walter Jones of the Air Force Office of Scientific Research.

References

[1] Wieghardt, K., "Hot Air Discharge for De-Icing," *Air Material Command*, AAF Trans. No. F-TS-919-RE, Dec. 1946.

[2] Hartnett, J. P., Birkebak, R. C., and Eckert, E. R. G., "Velocity Distributions, Temperature Distributions, Effectiveness and Heat Transfer for Air Injected Through a Tangential Slot into a Turbulent Boundary layer," *Journal of Heat Transfer*, Vol. 83, Aug. 1961, pp. 293–306.

[3] Tribus, M., and Klein, J., "Forced Convection from Non-Isothermal Surfaces," *Heat Transfer, a Symposium*, Univ. of Michigan Press, Ann Arbor, MI, 1953, pp. 211–235.

[4] Stollery, J. L., and El-Ehwany, A. A. M., "A Note on the Use of Boundary-Layer Model for Correlating Film Cooling Data," *International Journal of Heat and Mass Transfer*, Vol. 8, No. 1, 1965, pp. 55–65.

[5] Ballal, D. R., and Lefebvre, A. H., "Film Cooling Effectiveness in the Near Slot Region," *Journal of Heat Transfer*, Vol. 93, May 1973, pp. 165–166.

[6] Burns, W. K., and Stollery, J. L., "The Influence Foreign Gas Injection and Slot Geometry on Film Cooling Effectiveness," *International Journal of Heat and Mass Transfer*, Vol. 12, No. 9, 1969, pp. 935–951.

[7] Goldstein, R. J., "Film Cooling," *Advances in Heat Transfer*, Vol. 7, Academic Press, New York, 1971, pp. 321–378.

[8] Marek, C. J., and Tacina, R. R., "Effect of Free-Stream Turbulence on Film Cooling," NASA TN D-7958, 1975.

[9] Simon, F. F., "Jet Model for Slot Film Cooling With Effect of Free-Stream and Coolant Turbulence," NASA TP 2655, Oct. 1986.

[10] Lefebvre, A. H., *Gas Turbine Combustion*, Taylor & Francis, London, 1983, pp. 257–320.

[11] Zhou, J. M., Salcudean, M., and Gartshore, I. S., "A Numerical Computation of Film Cooling Effectiveness," *Near-Wall Turbulent Flows*, Elsevier Science Publishers, The Netherlands, 1993, pp. 377–386.

[12] Jansson, L. S., Davidson, L., and Olsson, E., "Calculation of Steady and Unsteady Flows in a Film-Cooling Arrangement Using a Two-Layer

Algebraic Stress Model," *Numerical Heat Transfer*, Vol. 25, Pt. A, 1994, pp. 237-258.
[13] Roy, S., Kapadia, S., and Heidmann J. D., "Film Cooling Analysis Using DES Turbulence Model," ASME Turbo Expo Paper GT 2003-38140, June 2003.
[14] Mehta, R. D., and Bradshaw, P., "Design Rules for Small Low Speed Wind Tunnels," *The Aeronautical Journal*, Vol. 73, Nov. 1979, pp. 443–449.
[15] Cruz, C. A., and Marshall, A. W., "Surface and Gas Phase Temperatures Near a Film Cooled Wall," AIAA Paper 2004-3654, 2004.
[16] Shaddix, C. R., "Practical Aspects of Correcting Thermocouple Measurements for Radiation Loss," Western State Section/The Combustion Institute, WSS/CI 98F-14, 1998.
[17] Modest, M. F., *Radiative Heat Transfer*, McGraw–Hill, New York, 1993, pp. 200–217.
[18] Marshall, A. W., "Effects of Jet Momentum Distribution on Combustion Characteristics in Co-Swirling Flames," Ph.D. Thesis, Univ. of Maryland, College Park, MD, 1996.
[19] Press, W. H., Teukolsky, S. A., Vetterling, W. T., and Flannery, B. P., *Numerical Recipes in Fortran*, 2nd ed., Cambridge Univ. Press, Cambridge, England, U.K., 1992, pp. 542–551.
[20] Launder, B. E., and Rodi W., "The Turbulent Wall Jet—Measurement and Modeling," *Annual Review of Fluid Mechanics*, Vol. 15, Annual Reviews, Inc., Palo Alto, CA, 1983, pp. 429–459.